Radio Science

RESEARCH ARTICLE
10.1029/2018RS006725

Statistical Analysis of TEC Distributions Observed Over South and Central America

J. Villalobos[1] and C. E. Valladares[2]

[1]Department of Physics, Universidad Nacional de Colombia, Bogota, Colombia, [2]Hanson Center for Space Sciences, The University of Texas at Dallas, Richardson, TX, USA

Key Points:

- Maps of Total ElectronContent show pronounced day-to-day variability and quite often a discontinuous equatorial anomaly
- An empirical numerical model that uses the K_p index, the solar flux, and the day of the year only account for 70% of the variability
- During disturbed magnetic conditions localized electric fields and neutral wind disturbances produce additional variability

Correspondence to:
C. E. Valladares,
cev160230@utdallas.edu

Citation:
Villalobos, J., & Valladares, C. E. (2020). Statistical analysis of TEC distributions observed over South and Central America. *Radio Science*, *55*, e2018RS006725. https://doi.org/10.1029/2018RS006725

Received 3 SEP 2018
Accepted 29 NOV 2019
Accepted article online 11 DEC 2019

Abstract Total electron content (TEC) values measured with several arrays of dual-frequency GPS receivers operating continuously and simultaneously at equatorial and low latitudes are used to construct regional maps of TEC over South and Central America and the Caribbean region. This extended database comprises TEC values collected by 126 stations that operated in South America in 2008, 181 stations in 2009, and 324 stations in 2010. The latter year includes GPS stations in Central America and the Caribbean region, extending the TEC coverage from the southern tip of South America to the northern boundary of Mexico (~30°N latitude). The TEC maps contain high (0.5° × 0.5°) spatial resolution and good (30 min) temporal resolution. The most prominent feature of these maps is the day-to-day variability that is observed during all seasons and under quiet and active magnetic conditions. Single station plots display TEC variations with time scales of few hours and the appearance of TEC enhancements near-midnight that can be accounted for by electric fields associated with disturbed magnetic conditions and the reverse fountain effect, respectively. To assess the TEC dependencies upon season, solar flux, magnetic activity, and local time over South and Central America, two statistical procedures were employed. First, we constructed monthly averages of TEC values along three field lines that intersect the magnetic equator at 70°, 60°, and 50°W longitudes that show a complex pattern of variability and symmetry/asymmetry of the equatorial anomaly depending on the season, the longitude, and the solar flux. Our second analysis consists of a non-linear least-square fit to simultaneously extract the solar flux, magnetic, and seasonal dependencies of TEC for each square cell (0.5° × 0.5°) of the regional maps and for each 30-min time sector. It is found that during low solar flux conditions, the anomaly is weak or non-existent. When the solar flux F10.7 index increases to 85 units the anomaly shows to be fully developed but contains a pronounced longitudinal/seasonal dependence. During the equinoxes and afternoon hours, the northern crest extends across the South American continent, but the southern crest prevails in the eastern side of South America. It is found that the non-linear numerical fitting of the TEC distributions can reproduce only 70% of the TEC variability.

1. Introduction

A salient feature of the low-latitude ionospheric variability is an enhancement of the plasma density that is observed at both sides of the magnetic equator. These enhancements have been called the Appleton (also named equatorial) ionization anomaly (EIA) (Appleton, 1946). The anomaly is also observable using latitudinal profiles of total electron content (TEC) gathered using a network of GPS receivers (Valladares et al., 2001). The anomaly is the result of the upward motion of the plasma near the magnetic equator and its consequent diffusion poleward along the magnetic field line (Hanson & Moffett, 1966) driven by pressure gradients and the gravity force (the fountain effect). During the day and early evening, the F-region plasma moves upward creating a density gradient along the field lines. The TEC anomaly starts to develop as early as 1100 local time (LT). It moves away from the equator with increasing local time, as the equatorial F-region moves to higher altitudes, reaching a maximum development around 2000 LT. After 2100 LT, the crests of the anomaly sometimes move toward the equator as the equatorial ionosphere moves downward. This latter process has been called "the reverse fountain effect" (Balan & Bailey, 1995; Sridharan et al., 1994). The reversal of the fountain is propelled by a flip of the sign of the pressure gradient force allowing the plasma to move upward and equatorward along the field lines. The presence of a meridional neutral wind blowing outward from the summer hemisphere will create an asymmetry in the amplitude of the crests with smaller densities on the downwind side (Valladares & Chau, 2012; Walker et al., 1994).

In addition to the equatorial anomaly, it has been suggested that the wavenumber 4 and planetary waves are a source of large-scale density variability (Sagawa et al., 2005). The far ultraviolet (FUV) images

introduced by Sagawa et al. (2005) revealed the existence of a four-node longitudinal structure in the latitudinal displacement of the EIA around the Earth. This effect was explained in terms of an eastward propagating (non-migrating) diurnal tide with zonal wavenumber 3 (DE3) excited by tropical tropospheric latent heat release (Hagan et al., 2007), resulting in modulation of the electric field in the lower ionosphere (Immel et al., 2006). The modulated electric field produces a wavenumber 4 longitudinal structure in the EIA region across the Earth when observed in a Sun-synchronous frame. These studies asserted the role of energy inputs from the lower atmosphere in producing day-to-day variability and indicated the importance of non-migrating tides. Other thermospheric sources of energy are planetary waves (PW) able to penetrate up to 100 km altitude that introduce multi-day periodicities by modulating tidal amplitudes (Fuller-Rowell et al., 2008).

This paper presents TEC values collected by several networks of GPS receivers that operated in South America between 2008 and 2010 and by over 100 GPS receivers installed in Central America and the Caribbean regions during 2010 to investigate the TEC variability and its dependence on the season and magnetic and solar activities. The years 2008 and 2009 were part of the solar cycle 23–24 minimum, which is considered to be one of the longest and deepest solar minima. During the 23–24 minimum, there were 266 spotless days in 2008, the most since 1913, and the Sun's brightness dropped by 6% at EUV wavelengths since the solar minimum of 1996, and the solar flux index (F10.7) was 69.7 units. In 2010 the solar flux index increased to an average value equal to 83.7 solar flux units (1 sfu = 10^{-22} W m^{-2} Hz^{-1}).

Section 2 of this paper gives a succinct description of the instrumentation that has been deployed in South America for the Low Latitude Ionospheric Sensor Network (LISN) effort. Section 3 provides TEC maps aiming to show the strong day-to-day and hour-to-hour variability of the equatorial and low-latitude ionosphere in the American sector. Section 4 describes the results of a statistical analysis of the regional TEC variability with the goal of finding the controlling parameters of this variability. Sections 5 and 6 are the discussion and conclusion sections.

2. On the LISN Observatory

LISN is a distributed observatory acting as a permanent array of instruments devoted to investigating the complex day-to-day variability and the extreme state of disturbance that occurs in the equatorial ionosphere nearly every day after sunset. This observatory provides nearly real-time measurements (nowcast) to the space weather community. The rationale of the need for real-time measurements is to develop a short-term (60 min) predictive model of the ionosphere (forecast) based on real-time data ingestion techniques. All the LISN instruments possess the capability to upload their real-time observables to a server that is located in Lima, Peru and to a second server that is located within the campus of the University of Texas at Dallas. The data acquired by LISN can be complemented with an assimilative physics-based model constrained with the multipoint and multi-instrument observations to produce accurate estimates of ionospheric electron density distributions, conductivities, E × B plasma drifts, and neutral winds in near real-time (Eccles et al., 2011, 2015).

The LISN observatory consists of three different types of instruments: GPS receivers, flux-gate magnetometers, and Vertical Incidence Pulsed Ionospheric Radar (VIPIR) ionosondes. LISN presently manages 35 GPS receivers, six magnetometers, and four VIPIR ionosondes. The GPS receivers were deployed across the South American continent with an emphasis to fill regions devoid of GPS receivers. Figure 1 shows the location of 300+ GPS receivers (in red) that operated in South and Central America and the Caribbean region in 2010. The magnetometers operate forming two latitudinal baselines (Figure 2a) at the center of South America. The western baseline is near 69°W (Puerto Maldonado–Leticia–Tucuman–El Leoncito), and the second one is close to 56°W (Alta Floresta–Cuiaba). The ionosonde network consists of four VIPIRs installed at Tucuman, Tupiza, P. Maldonado, and Jicamarca. These VIPIR ionosondes operate continuously with a 1–2 min cadence time for a full ionogram scan (1.5–20 MHz). The observatory also includes an archival data system to store all the historical data collected with the LISN GPSs, magnetometers, and VIPIRs. Several data sets are made public via the web page at http://lisn.igp.gob.pe/.

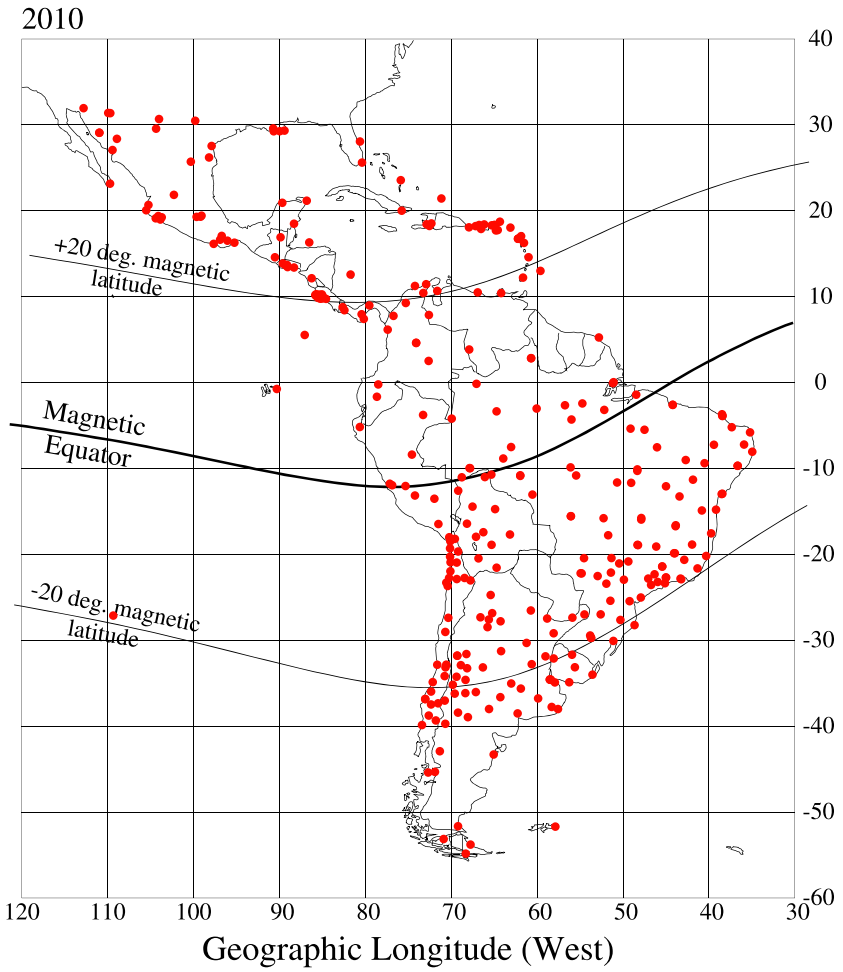

Figure 1. Location of GPS receivers that belong to several networks (red dots) that operated in South and Central America and the Caribbean region in 2010.

3. TEC Variability Over South America

A calculation of TEC values was conducted following the guidelines outlined by Rideout and Coster (2006). The maps of TEC over South America were constructed following the method discussed by Valladares and Chau (2012). This section presents the extreme variability that affects the low-latitude ionosphere in a day-by-day and on an hour-by-hour basis. This variability is produced by changes in the solar zenith angle, season, magnetic activity, solar cycle, and the fountain effect; other physical mechanisms modify and perturb the TEC distributions. Processes such as equatorial plasma bubbles (spread F), localized zonal electric fields, meridional neutral winds, the reverse fountain effect, gravity waves, and intensifications of a semidiurnal tide introduce a temporal and spatial variability. However, we still do not have a full understanding of the appearance and development of some of these processes, much less the ability to forecast the low-latitude ionospheric densities.

Figures 3 and 4 display TEC values measured by several GPS networks that operate in South America. Figure 3 shows a map of TEC values measured over South America in which a continuous and symmetric anomaly was observed on two consecutive days: 21 and 22 October 2009. The EIA consists of an increase in TEC directly associated with the fountain effect. The increase can be symmetric or asymmetric with respect to the magnetic equator. The anomaly extends across the continent almost unchanged in spite of the local time variation between 12 and 16. The formation of the anomaly is driven by an upward vertical drift near the magnetic equator followed by plasma diffusion down the field lines. The continuous and quite symmetric nature of the TEC anomaly suggests the presence of a constant and longitudinal invariant electric field

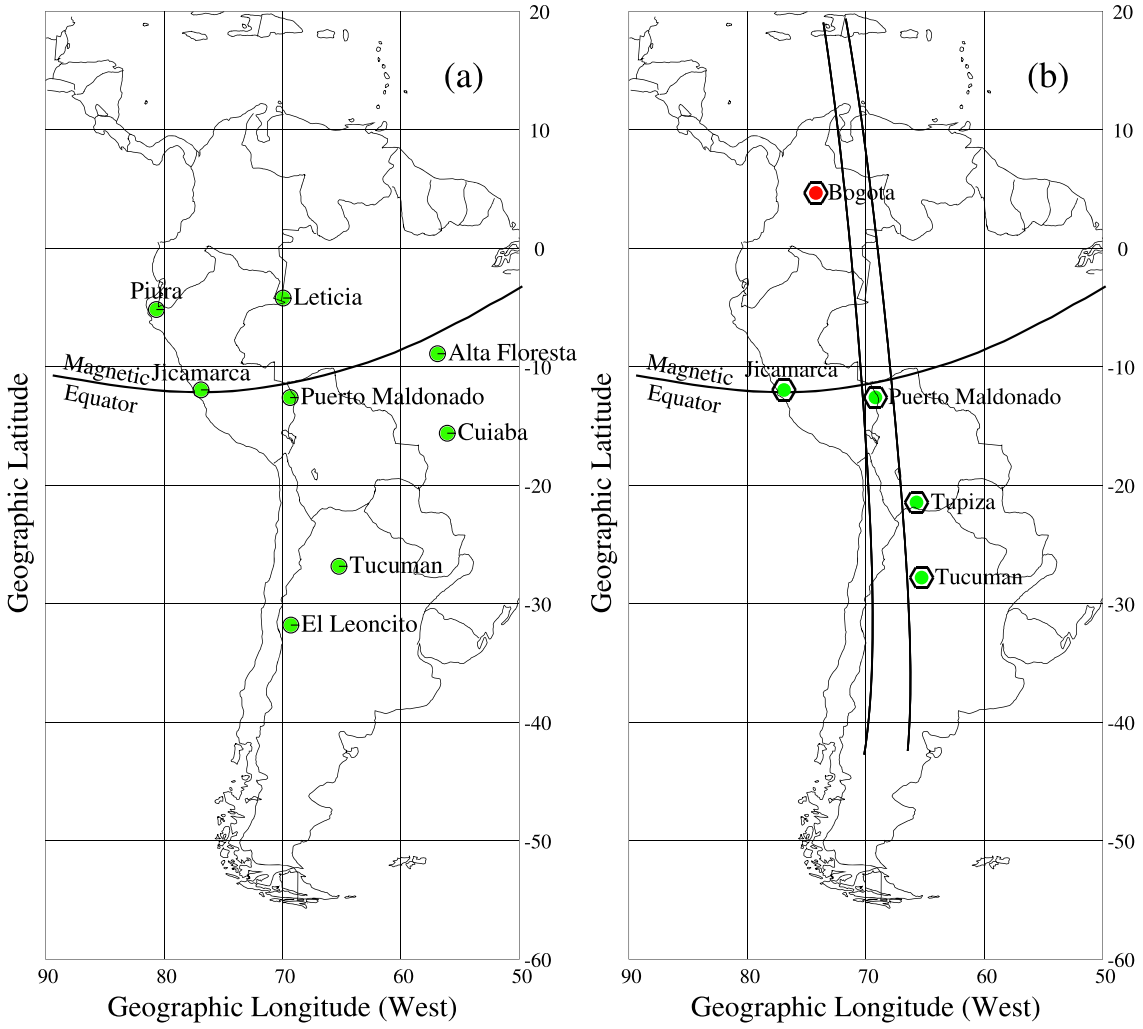

Figure 2. Panel (a) displays the geographic location of the LISN magnetometers in South America (Puerto Maldonado, Leticia, Alta Floresta, Cuiaba, and El Leoncito) forming two baselines near the center of the South American continent. The third baseline of two magnetometers exists in the Peruvian sector (Jicamarca and Piura). Panel (b) shows the geographic location of four VIPIRs (in green) presently operating in South America and one more (in red) to be installed in September 2019. The parallel lines near 70°W meridian represent the ground projections of two magnetic field lines that intersect the magnetic equator at 70° and 72°W longitude.

across the continent and an almost absent meridional wind. It is important to mention that a symmetric and continuous TEC distribution is not a typical display in the TEC database for the years 2008, 2009, and 2010.

All three frames of Figure 4 correspond to the same universal time (UT) but were observed on three consecutive days between 15 and 17 October 2008 during a period of quiescent magnetic conditions (K_p values = 1^-, 0^+, and 1^-). This figure illustrates the extreme day-to-day and spatial variability that the TEC distribution presents over extended regions. The left frame displays an asymmetric anomaly that has a dominant crest located north of the magnetic equator in the western side of the continent and south of the equator in the eastern side of South America. The central panel shows the anomaly terminating near 60°W longitude, coinciding with an intrusion of TEC from the northern crest toward the magnetic equator at 65°W. The right frame, corresponding to 17 October, shows the southern crest extending across the continent and a northern crest confined to the western side. We conclude that between 15 and 17 October 2008, the day-to-day variability of the TEC distribution was very intense, but the spatial scale of this variability was fully embedded within the South American continent and well diagnosed by the GPS receivers. It is suggested that the spatial and temporal variability of the anomaly is a direct effect of highly variable zonal electric fields and meridional winds that are likely confined in longitude.

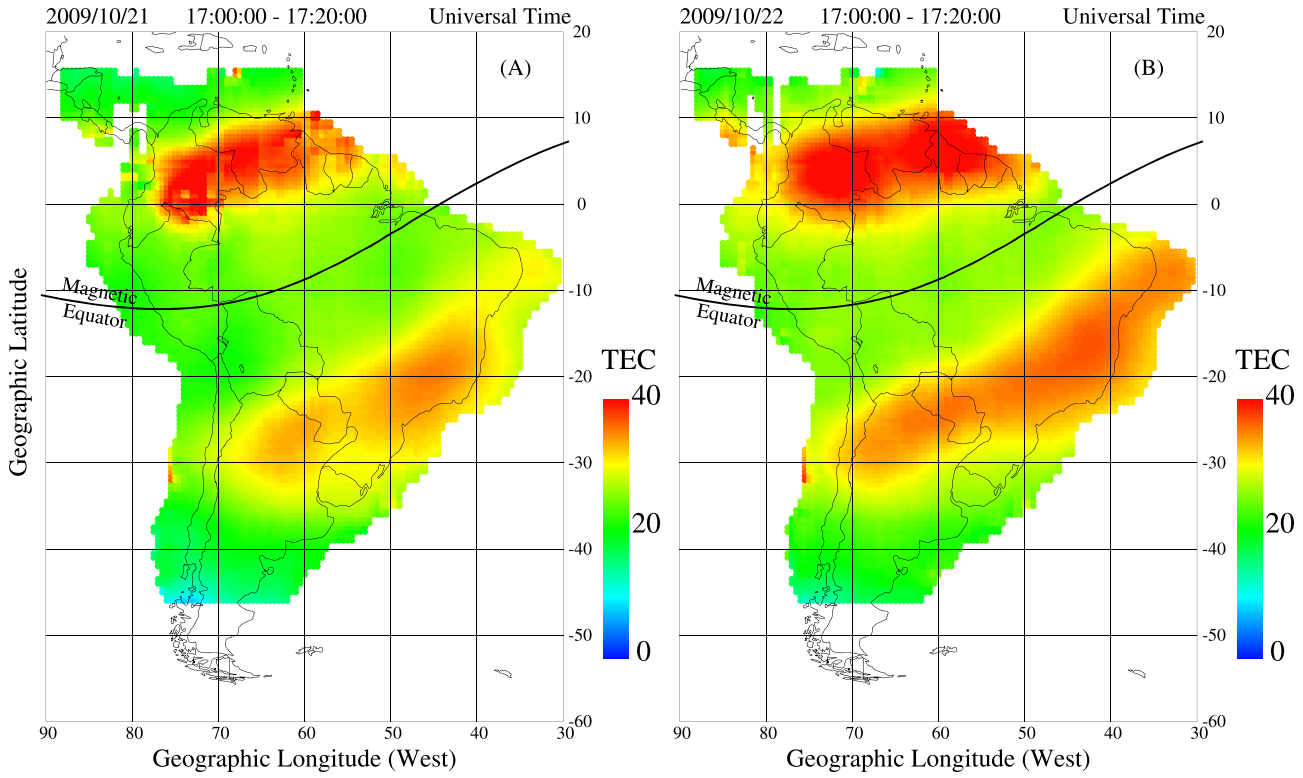

Figure 3. Reconstructed maps of TEC values for 21 and 22 October 2009 corresponding to 1700–1720 UT time interval. Typical anomaly configurations were observed on both consecutive days.

3.1. Hour-by-Hour TEC Variability

Figures 5 shows a sequence of TEC distributions measured over South America on 14 October 2010. During these observations, the magnetic conditions were quiet ($K_p < 1^-$), and the solar flux was equal to 79.9×10^{-22} W m^{-2} Hz^{-1}. This figure and the next two show TEC values measured every hour between 12 and 24 UT using an average of 180 GPS receivers. More details on the TEC calculations and the fitting algorithm for

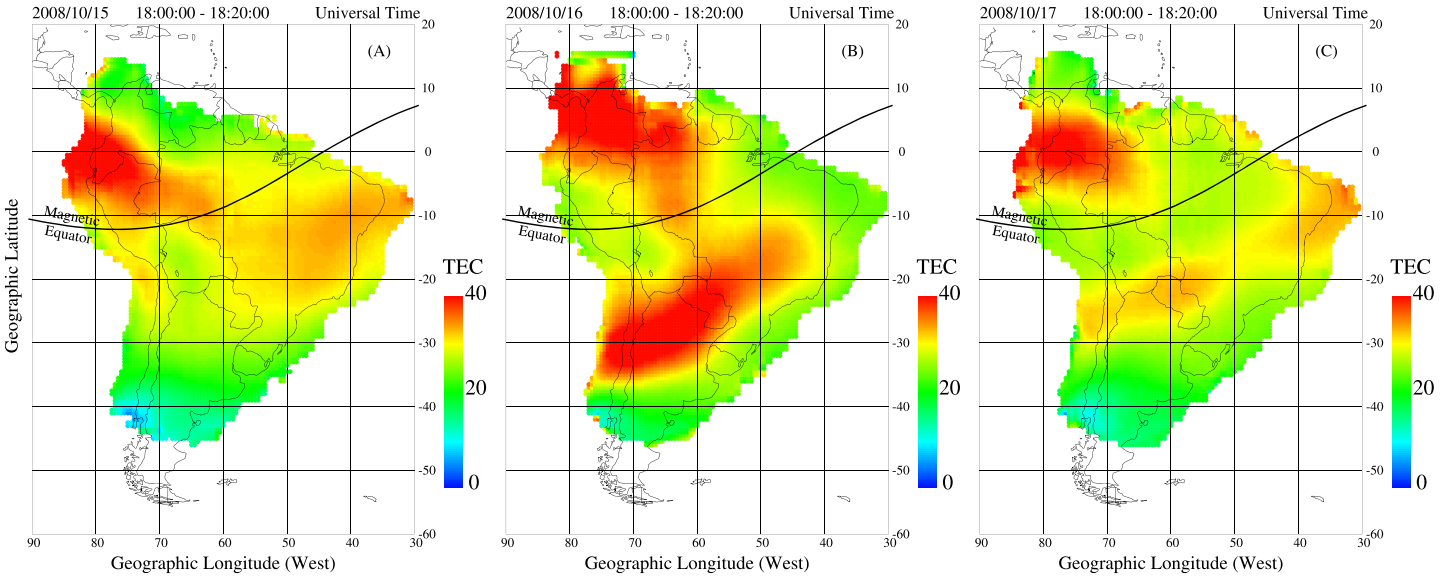

Figure 4. Non-typical TEC distributions observed on three consecutive days (15–17 October 2008). The symmetry and asymmetry of the EIA crests vary during these three consecutive days.

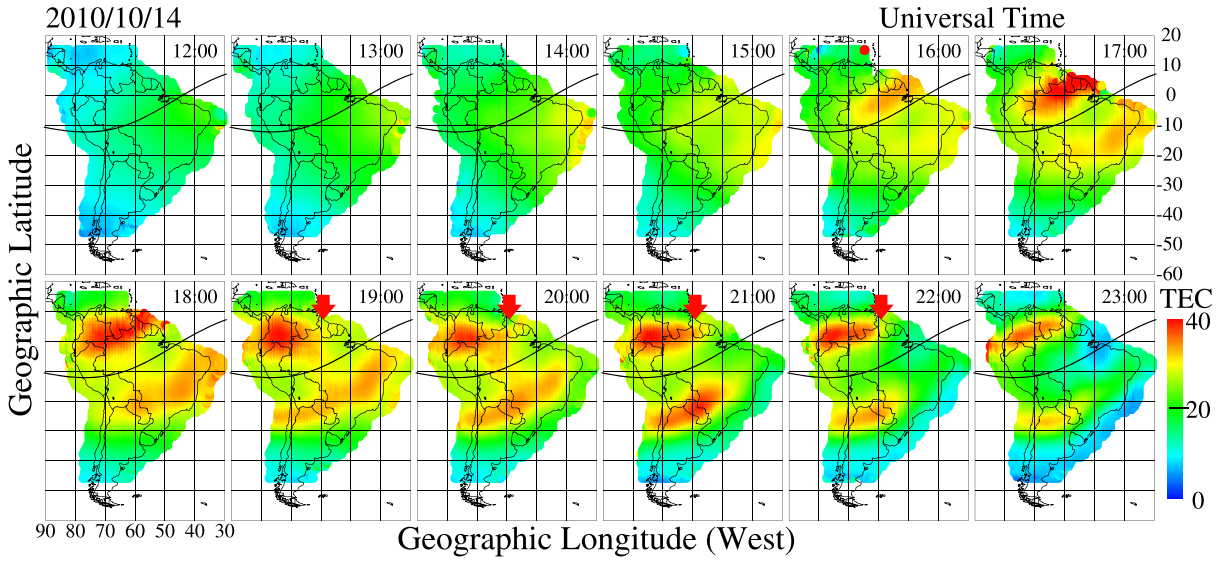

Figure 5. TEC values over South America measured every hour on 14 October 2010. Note the westward shift of the EIA and later the discontinuity of the northern crest at 60°W (red arrow). The red arrows indicate the eastern end of the northern crest of the anomaly. Between 18 and 20 UT, the southern crest of the anomaly extends all across the South American continent but shortens after 20 UT.

the TEC interpolation can be found in Valladares and Chau (2012). The anomaly starts forming at 14 UT (~12 LT at 30°W) and intrudes westward following the Sun's migration during the next 2 hr. After 17 UT the anomaly develops a north-south asymmetry presenting a more pronounced northern crest. The northern crest also shows a discontinuity near 60°W that lasts for several hours (see red arrows). The anomaly recovers its symmetry at 21 UT but asymmetrically decays after 23 UT. Based on our TEC values for 2008–2010 and the high temporal, and spatial variability, the TEC profiles observed on 14 October can be considered to be quite typical for an equinoctial day. The following two figures show a strong hour-by-hour variability.

On 2 June 2010 the magnetic conditions were quiet ($K_p < 2^o$), and the solar flux was 76.1×10^{-22} W m^{-2} Hz^{-1} (Figure 6). This figure displays the formation and evolution of the anomaly during a typical June solstice

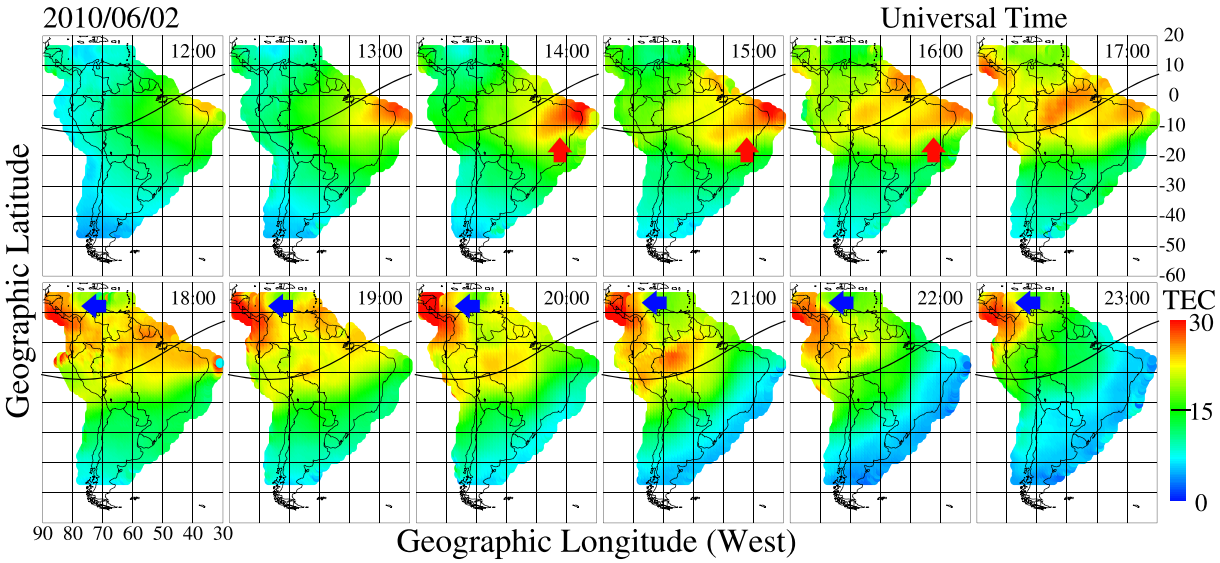

Figure 6. Same as Figure 5, but for 2 June 2010. Note the small separation of the anomaly in the Brazilian sector between 14 and 18 UT. Blue arrows point to the location of a TEC enhancement over Central America between 18 and 23 UT. Red arrows indicate the location of the vanishing southern crest of the anomaly.

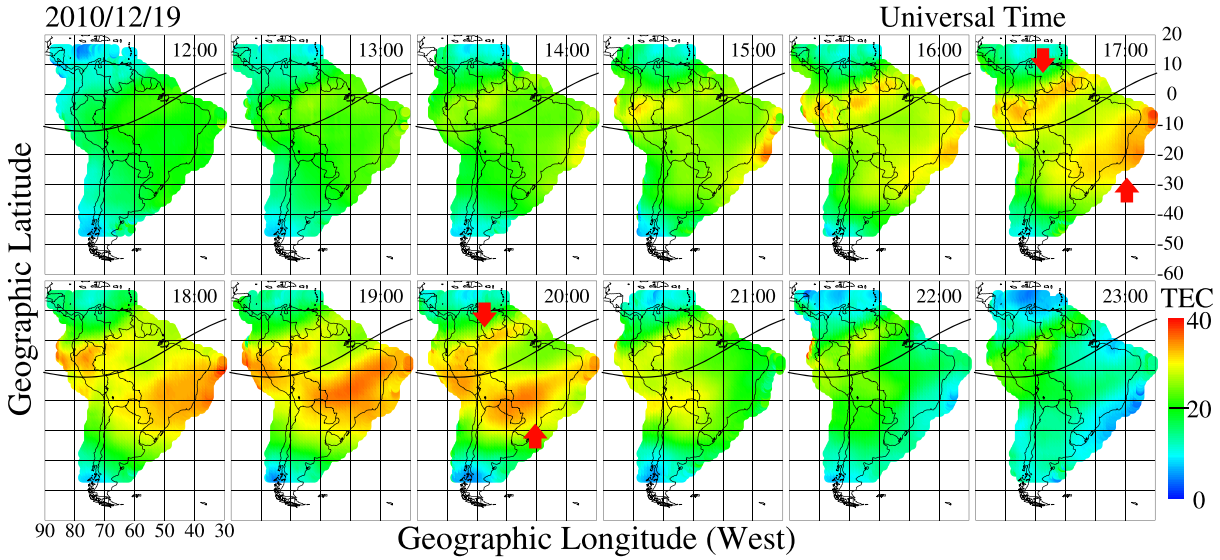

Figure 7. Same as Figure 5, but for 19 December 2010. The anomaly is fully developed over the Brazilian sector but almost non-existent in the Peruvian region. Red arrows (at 17 and 20 UT) show the locations of both crests of the equatorial anomaly that developed in the eastern part of South America.

magnetically quiet day. The onset of the anomaly occurs in the early morning (13 UT), but only the southern crest shows an elevated value that is confined to the Brazilian sector (see red arrows between 14 and 16 UT). In addition, the latitudinal separation of the crests of the anomaly from the magnetic equator (as seen at 17–18 UT) is less than 10°. This small separation is quite typical for South America during the June solstice season when small electric fields are prevalent (Fejer et al., 1999). It is important to mention that near 18 UT, there exists a region over Central America where high TEC values persist for several hours (see blue arrows). These high TEC values have been observed on several occasions; they typically develop between June and October months. It is also indicated here that the highest TEC value measured on this day over the American sector was not encountered near the equator or at low latitudes but over the country of Honduras at magnetic latitude larger than 20°.

Figure 7 presents the TEC values measured on 19 December 2010, in which the magnetic conditions were quiet ($K_p \leq 1^+$) and the F10.7 solar flux equal to 87.3×10^{-22} W m^{-2} Hz^{-1}. It has been demonstrated before that during the December solstice the electric fields are better developed over the Brazilian sector, where the magnetic meridian aligns more with the terminator than in the Peruvian sector (Fejer et al., 2010; Pacheco et al., 2010). This idea is evident in Figure 7 where there exists a marked longitudinal variability in the latitudinal separation of the crests of the anomaly. The anomaly is well developed over the eastern part of Brazil where the separation exceeds 12° (red arrows at 17 and 20 UT). The anomaly separation diminishes toward the west and reduces to almost zero in the western part of Brazil. Further west, over the Peruvian sector the anomaly is non-existent as the maximum TEC values reside over the magnetic equator. The TEC plot corresponding to 21 UT shows the anomaly to emerge in the Peruvian sector but decaying before sunset (23 UT).

3.2. TEC Variability as a Function of Longitude and Latitude

This section presents TEC values recorded over a dozen stations during 2 days in which disturbed conditions prevailed, drastically modifying the daily pattern of TEC values. The K_p value was equal to 5^- at the beginning of both days. There are two types of events: (1) near-midnight TEC enhancement and (2) a period of magnetically disturbed conditions that developed when South America was in the dayside sector. Figure 8 shows 24-hr plots of TEC values recorded at 12 individual stations on 12 March 2011. The left panel shows the geographic locations for each station indicated using large red dots. The selected stations are aligned from north to south along three magnetic meridians that cross the eastern side of Peru, the western and the central Brazilian sectors. Their corresponding TEC plots are organized in a similar pattern. The different traces seen in all frames correspond to the TEC values observed using signals from different GPS satellites.

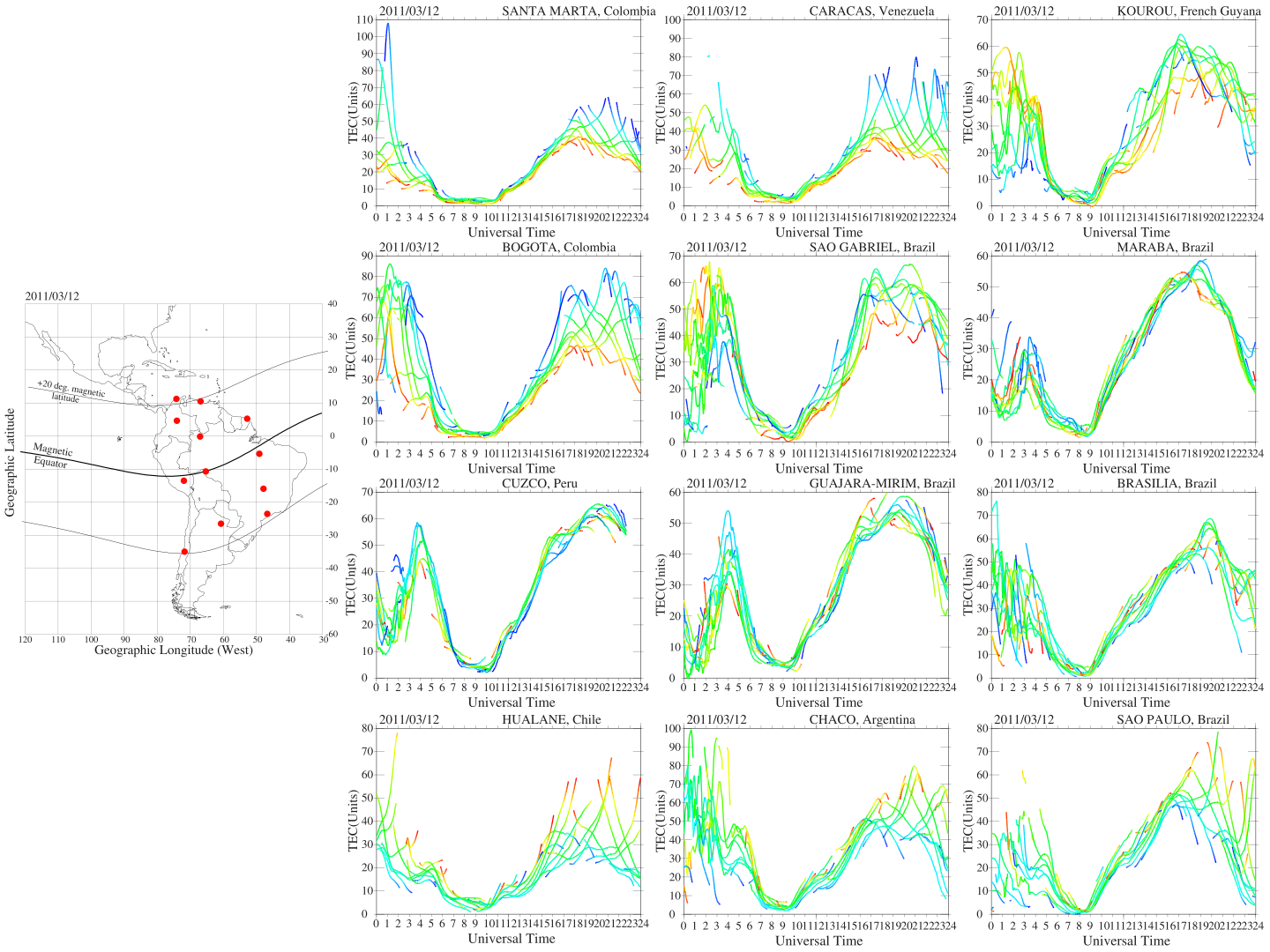

Figure 8. 24-hour plots of TEC values recorded over a dozen stations in South America on 12 March 2011. The left frame shows the geographic location of each site. Note the large daily variability of the TEC values. TEC varies between two TEC units at 07 UT and ~60 TEC units at 19 UT. The colored traces point out the latitude where the TEC measurements have been conducted. Red color indicates northward distances with respect to the station latitude. Blue color displays southward locations. LT = UT + longitude/15.0.

The four frames in the left column show from top to bottom 24-hr plots of TEC for the stations of Santa Marta, Bogota, Cuzco, and Hualane. TEC values from Santa Marta (magnetic latitude = 20°) show a rapid decrease in TEC that occurred right after sunset (01 UT). Bogota, located 6° south of Santa Marta, also shows a TEC decrease that starts at 03 UT and ends near 05 UT. At Cuzco, located close to the magnetic equator (magnetic latitude = −1.5°), there exists an anomalous TEC enhancement of ~45 units that last for several hours centered slightly before midnight (05 UT) when there is no EUV ion production. This resurgence of the TEC called the near-midnight TEC enhancement, manifests as a sudden rise of the TEC values near 20 LT (01 UT), a peak close to 23 LT (04 UT), and a decay after 24 LT (05 UT) (Balan & Bailey, 1995). A minimal TEC enhancement of ~3 TEC units is observed at Hulane located at 23° magnetic latitude.

The second column of 24-hr plots of Figure 8 shows similar patterns of TEC decay and near-midnight (05 UT) enhancements. The stations placed near the magnetic equator display (e.g., Sao Gabriel and Guajara-Mirim) large TEC enhancements that occur between 02 and 06 UT, and the stations located under the crests of the anomaly present rapid post-sunset (01 UT) decays. The station of Maraba, located 2° south of the magnetic equator, shows a smaller TEC enhancement, illustrating a reduction in the amplitude of the near-midnight TEC enhancement at longitudes located further east.

During this day, several stations presented sudden increases in the local TEC values that occurred 2–3 hr after sunset and extended for a few hours before and after midnight. It is suggested that near-midnight TEC enhancements are produced by the transport of plasma along field lines from latitudes larger than 16° toward equatorial latitudes, by a process that is called the reverse fountain effect. It is also indicated that the presence of a meridional wind can modify the final location of the region of enhanced TEC values. The TEC enhancement, seen on 12 March 2011, is the largest event ever recorded in South America using GPS receivers. It is expected that as we move into the period of maximum activity of the present solar cycle, much larger near-midnight TEC enhancements will be detected.

Figure 9 illustrates the effect produced by prompt penetration electric fields on the dayside low-latitude ionosphere during the magnetic storm of 5 April 2010. The magnetic K_p index was 5^+ at 09 UT and rose to 8^- at 12 UT. This figure has the same format as Figure 8 with the left frame containing the locations of 12 stations grouped along three magnetic meridians. Note that TEC values from one station located as far north as Mayaguez in Puerto Rico and another placed as far south as Bahia Blanca in Argentina are included in this analysis. Right after sunrise (11 UT), the TEC values start increasing due to the solar EUV radiation initiating earlier at eastern longitudes. On quiet days, the TEC increase continues during the morning hours (13 UT) until a maximum is attained in the early afternoon typically occurring ~14 hr local time (19 UT at 75°W).

On 5 April 2010, each of the 24-hr plots of Figure 9 indicates that the morning TEC rise was interrupted approximately at 13 UT by a prompt penetration electric field that modified the electrodynamics of the ionosphere. A westward electric field can make the ionosphere move downward, enhancing recombination and accelerating the decrease of the TEC values. Abdu et al. (2008) found large decreases in the f_0F_2 due to the development of prompt penetration E fields during the superstorm of 30 October 2003. Some of the frames of Figure 9 present a sudden TEC decrease; in other cases, there exist only a flattening of the TEC traces (e.g., Bogota and Sao Gabriel). The stations at higher latitudes, Concepcion, Chile, Bahia Blanca, Argentina, and Barbados, USA, show a pronounced TEC decrease as high as 10 TEC units. Equatorial stations like Cuzco in Peru and Alta Floresta in Brazil show only a reduced growth that lasts for few hours. The stations located further east, like Alta Floresta, Guarapuava, and, Ilha Solteira, all of them in Brazil, also show a second flattening of the TEC values that occur at 10 UT. The TEC decrease occurs 3 hr prior to the decrease of 13 UT. The prompt penetration electric field of 10 UT was not evident in the stations located west of 58°W because the local sunrise occurred after the initial onset of the electric field, and the local density was quite small to indicate any increase or decrease. A more careful study should be able to identify the magnitude, the spatial extension, and the direction (zonal vs. meridional) of the electric fields that are producing these TEC changes. This investigation is beyond the scope of the analysis conducted here.

4. Statistical Analysis of TEC Variability

Section 3 has shown the pronounced day-to-day and seasonal variability of the TEC regional patterns. This variability is contained within the South American continent with a spatial coverage on the order of thousands of kilometers and temporal variability on the order of 1 hr. This section describes the dependence of this variability upon the seasons, the magnetic conditions, and the solar flux. First, we introduce the seasonal variability of TEC values along three magnetic meridians that are separated by 10° in longitude. Second, we present the results of an empirical model that includes the dependencies on solar flux, magnetic conditions, and season of the TEC values over South and Central America. Section 4.3 presents residual TEC values; this is the difference between measurements and empirical model. Residual TEC patterns are shown for two consecutive days.

4.1. Seasonal TEC Variability

Monthly averages of the TEC values measured over South America were calculated along three magnetic meridians that cross the magnetic equator at 70°, 60°, and 50°W longitudes. The TEC values along these magnetic meridians are portrayed as a function of latitude and universal time in the three panels of Figures 10–13. Figures 10–13 correspond to the months of March, June, September, and December, respectively. The white lines indicate the location of the magnetic equator as this varies in all longitudinal sectors. We have also derived similar plots for the years 2008 and 2010 and for each month of the year. We found

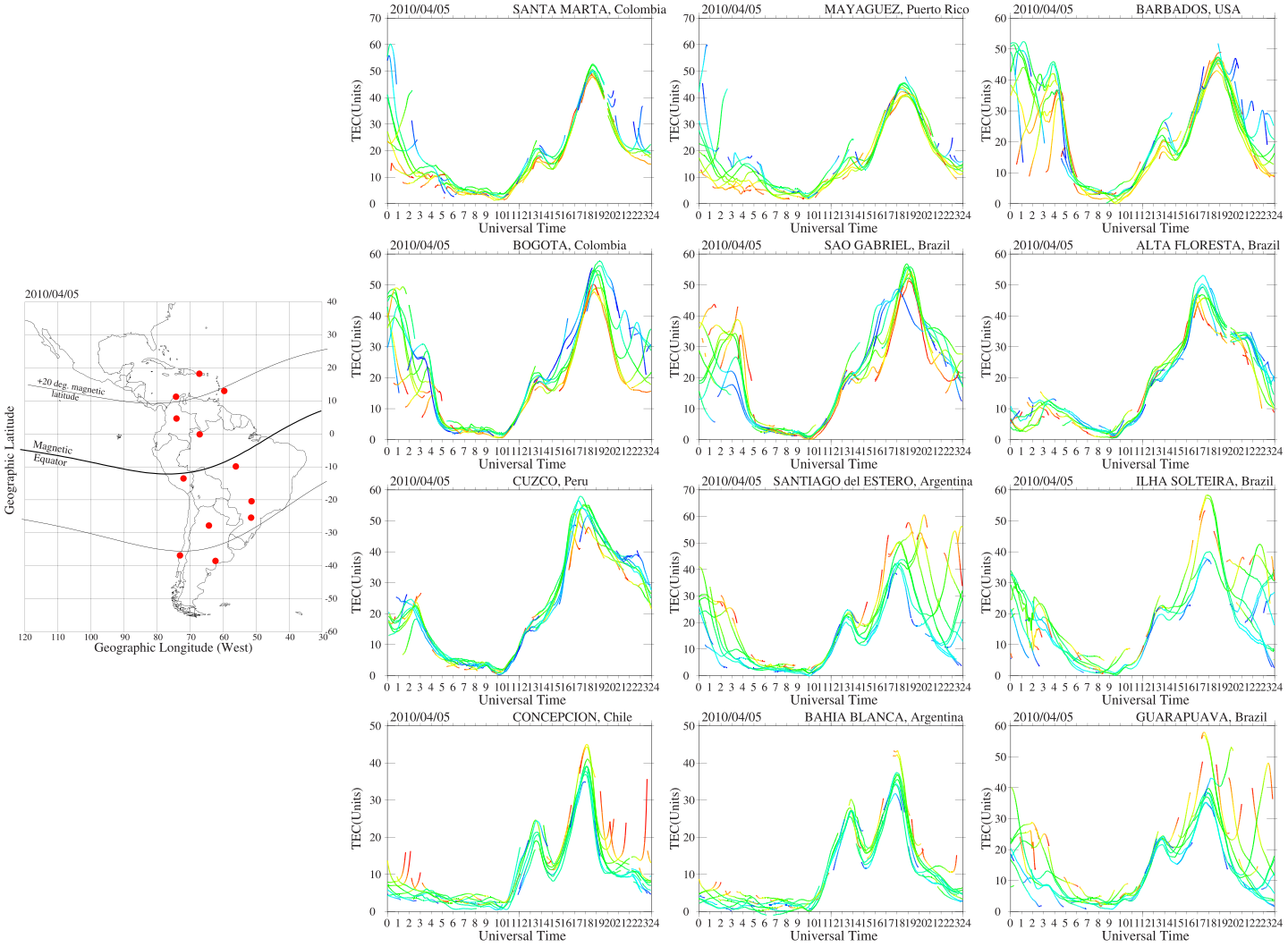

Figure 9. Same as Figure 8, but corresponding to 5 April 2010. Note the TEC variability during daytime hours seen at all the stations. The TEC variability is produced by electric fields during a magnetic storm. The prompt penetration of the electric field into the low latitude ionosphere produces significant TEC variability. One of these variations is evident at 13 UT when TEC decreases by 10 TEC units.

almost no morphological changes in the symmetry and duration of the anomaly for the two other years and for other months not displayed here.

Section 3 pointed out the profound asymmetry that was found quite often between the northern and southern crests of the anomaly. Here, we introduce the average TEC values that were derived, adding month-long TEC series without attention to the solar and magnetic conditions to determine the seasonal changes of the TEC distributions. It is evident that the anomaly symmetry/asymmetry characteristics that are seen daily persist throughout the year, and the general trend of the seasonal/longitudinal dependence remains. In March 2009 (see Figure 10) the anomaly is highly asymmetric at 70°W. In fact, the southern crest is nonexistent in the top panel. The intensity and the extension of the southern crest increase at the 60° magnetic meridian making the anomaly to become almost symmetric along the 50° longitude magnetic meridian. The peak of the northern crest is displaced 10–12° from the magnetic equator. This value is quite typical for a year of minimum solar activity. It is important to note that at longitudes near 50°W, the extension of the field line over the continent is shorter than at further west longitudes, consequently reducing the field of view in this sector to latitudes between 6° and −30° geographic latitude.

Figure 11 displays the average TEC values for the month of June 2009. All three panels show an asymmetric anomaly in which the southern crest is absent. In addition, the TEC values for June are 40% less than the

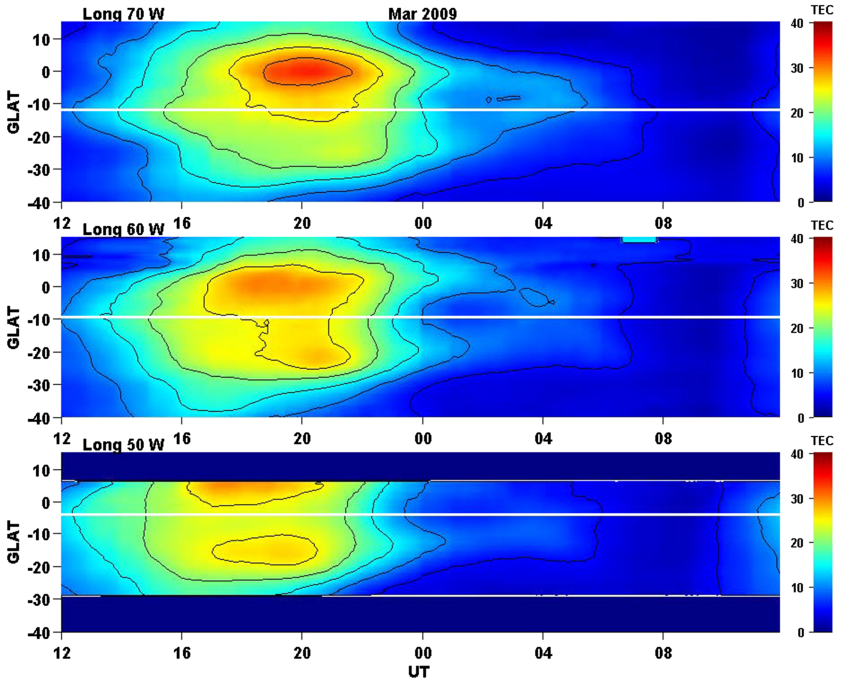

Figure 10. TEC values along three field lines averaged throughout the month of March 2009. The three panels correspond from top to bottom to field lines that cross the magnetic equator at 70, 60, and 50°W. The lower panel displays TEC values above 6° and below −30° latitude that are equal to zero due to the lack of GPS data outside South America.

TEC values for all other seasons. It is interesting to note that the displacement of the northern crest in the top panel is about 18°, decreases to 12° in the middle, and to 10° in the lower panel. This fact illustrates the high degree of variability across different longitudes that exist in the averaged TEC values.

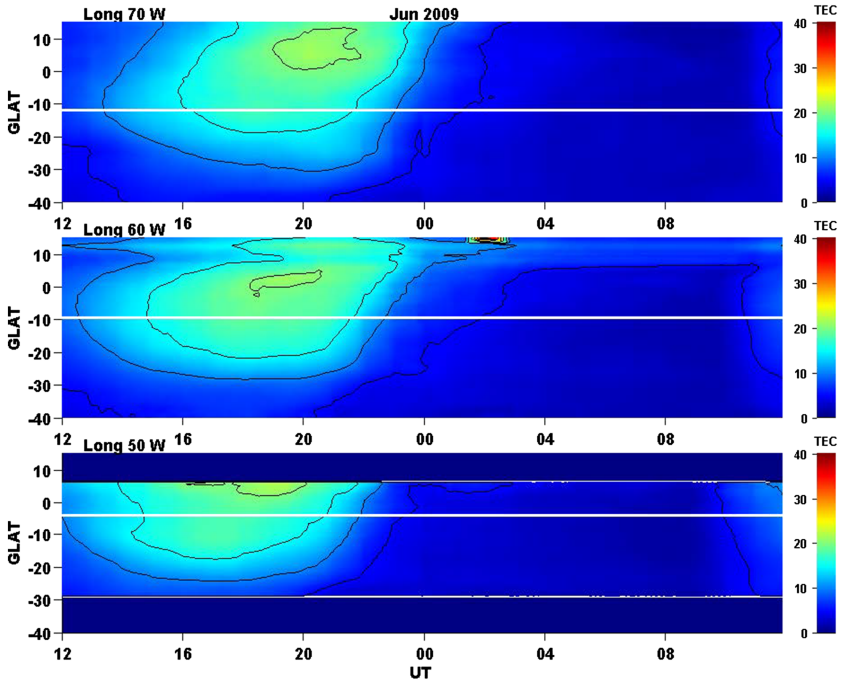

Figure 11. Same as Figure 10, but for the month of June 2009. Note the small TEC values during the June solstice over South America. Variability of the equatorial anomaly similar to the anomaly symmetry observed during the March Equinox (Figure 10).

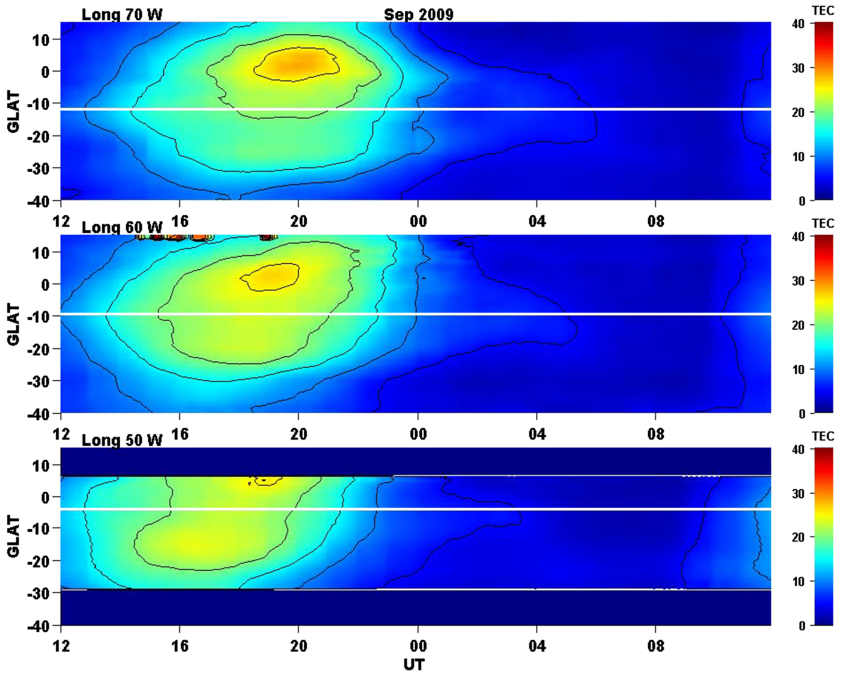

Figure 12. Same as Figure 10, but for the month of September 2009. Note the asymmetry of the EIA that contains a dominant northern crest. Variability of the equatorial anomaly similar to the anomaly symmetry observed during the March Equinox (Figure 10).

During the month of September 2009 (Figure 12), the symmetry of the crest of the anomaly varies for the eastern longitudes in a manner similar to Figure 10. The southern crest of the anomaly was absent at 70°W, but the EIA crests became almost symmetric at 50°W. The anomaly peak TEC value in September 2009 is less (30 TECu) than the maximum values detected in March 2009 (40 TECu) as seen in Figure 10.

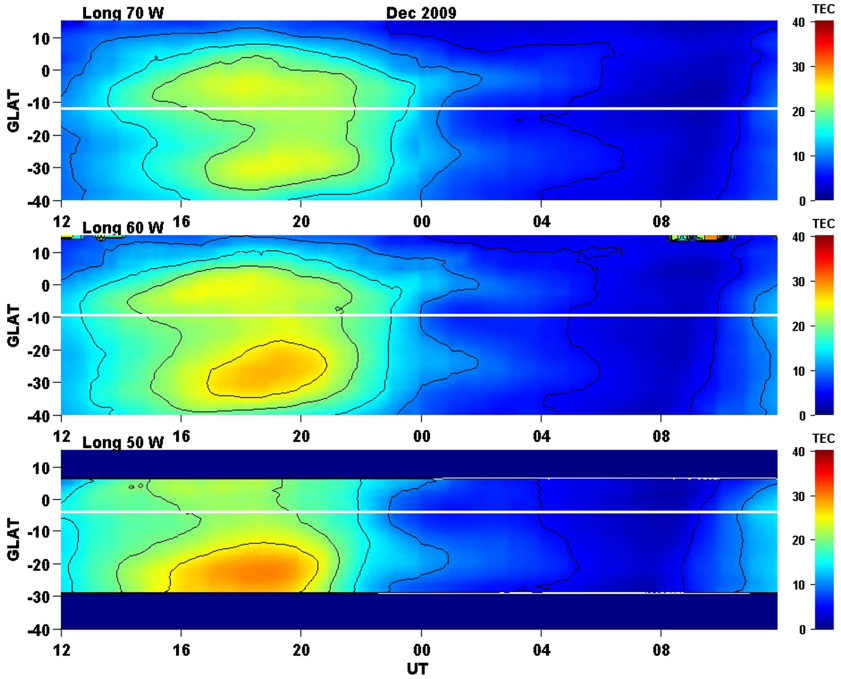

Figure 13. Same as Figure 10, but for the month of December 2009. Note the dominant southern crest of the EIA. Significant changes in the amplitude of the southern crest of the equatorial anomaly, becoming more prominent at 50°W and asymmetric.

Figure 13 shows the average TEC values observed in December 2009. The anomaly is symmetric at 70°W with peak values near 25 TEC units. At 60°W, the southern crest increases in size and becomes the dominant feature in this plot. The asymmetry is quite significant at 50°W, where the amplitude of the southern crest increases and the displacement from the magnetic equator becomes more pronounced.

4.2. Empirical Model of the TEC Variability as a Function of Season, Solar Flux, and Magnetic Activity

To elucidate the factors that control TEC distributions, we have used regional maps of TEC values gathered between 2008 and 2010 and derived the seasonal, solar flux, and magnetic dependence of the TEC values. These years are basically of low solar activity. Therefore, our calculations are restricted to low levels of the solar flux F10.7 index between 65 and 90 units. Several authors have addressed the influence that the solar flux, the magnetic activity, and the seasons have on the TEC variability. Walker et al. (1994) used TEC latitude profiles obtained in Southeast Asia to indicate that the amplitude of the TEC anomaly increased as a function of the solar radiation flux. Mannucci et al. (2005) suggested that during active magnetic conditions, penetration electric fields lead to increases in the ionospheric density by raising the layer height; these electric fields modify the fountain effect at the equator and transport the crests of the equatorial anomaly poleward. Khadka et al. (2016)) presented TEC latitude profiles obtained in the Peruvian sector to show the existence of a prominent annual variation containing a TEC peak in March and a minimum in August. Due to these observational facts and TEC measurements presented in sections 3 and 4, expression (1) has taken the following form.

$$TEC = (1 + \text{solar flux}) \times \left(1 + K_p + {K_p}^2\right) \times \left(1 + \text{DOY} + \text{DOY}^2 + \sin(2\,\pi\text{DOY}/365) + \cos(2\,\pi\text{DOY}/365)\right). \quad (1)$$

Expression (1) considers a linear dependence for the solar flux, a quadratic trend for the K_p index, and the combination of a quadratic and a sinusoidal variability for the DOY (day of the year). We least-square fitted expression (1) to a 3-year time series composed of 1,096 TEC values that correspond to each day of the 3-year period. This procedure was independently conducted for each pixel cell and for each 30-min frame of the TEC maps. The pixel size is about 0.5° × 0.5° in latitude and longitude. A total of 30 coefficients were individually calculated for each of the ~15,000-pixel cells and for each of the 48 30-min time intervals. This approach allows us to keep seasonal (day of the year) and universal time (hours) scales as independent variables.

It was found that for low K_p values ($<2^-$) and low solar fluxes (~65 units), the empirical model of TEC values presents small variability as a function of season and local time. We also observed that the anomaly is weakly developed under those conditions. For a solar flux equal to 85 units or higher, the TEC model displays single- and double-crest anomalies with characteristics that vary as a function of season and longitude. Figures 14–16 show TEC values for 12 consecutive hours between local noon and midnight that were calculated using the empirical model described above and for the conditions (day of the year, K_p, and solar flux) indicated in each figure. Figures 14 and 16 show well-defined and almost symmetric anomalies. In both figures, there exists a dominance of the northern crest, a faster decay of the southern crest in the late afternoon hours, and peak amplitudes in the eastern side of the southern crest larger than in the western part of South America. The modeled TEC distribution of Figure 16, corresponding to 22 September, display all the characteristics of a "classical" anomaly, with values 20 TEC units higher than the TEC encountered at poleward latitudes and a deep trough at the magnetic equator.

Figure 15 (21 June) shows maps of modeled TEC values in which an "apparent" northern crest of the anomaly appears at a very unusual latitude. This "apparent" northern crest is wide, extends to magnetic latitudes >25°, and presents a sharp termination at 80°W. In the western side of the TEC enhancement, the peak is placed above 20° magnetic latitude over Central America and seen to extend westward beyond the limits of the field of view of the GPS receivers that operate in Central America. In the eastern side, the northern crest is placed near the magnetic equator or few degrees away from the magnetic equator. The region of high TEC values over Central America persists for several hours during the afternoon hours but increases in magnitude and propagates to poleward latitudes as the K_p index augments. Valladares et al. (2017) presented TEC maps from Central and North America during the magnetic storms of 3 August 2010 and 5 August

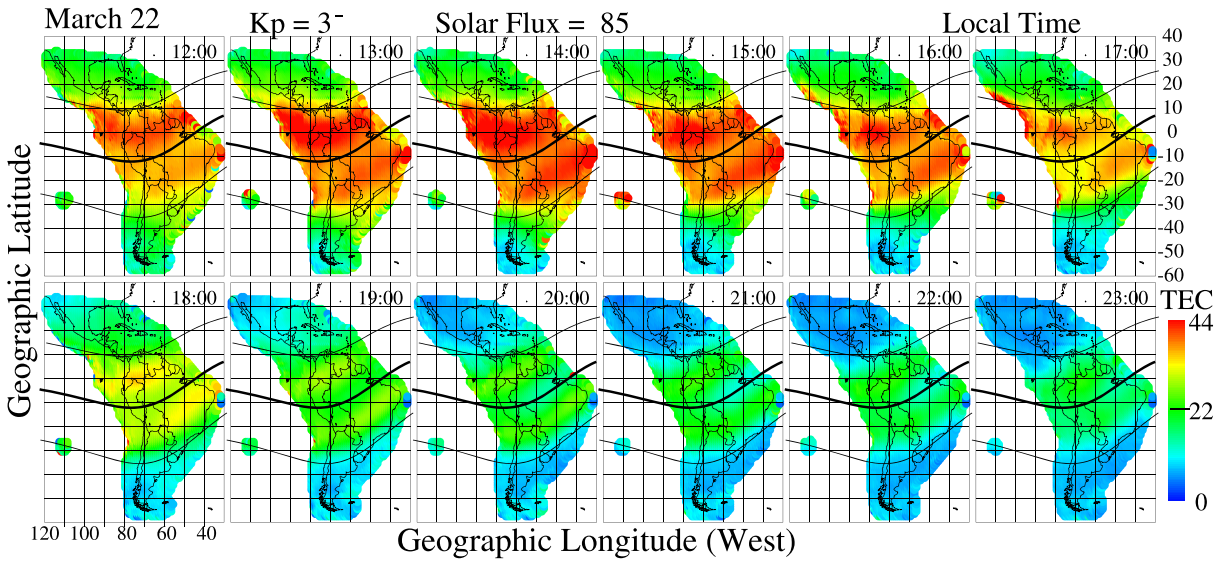

Figure 14. TEC values over South and Central America for 12 consecutive hours between local noon and midnight. The TEC values were provided by the empirical model and using the day of the year, K_p index, and solar flux indicated in the figure. See text for details.

2011. These authors also observed a region of high TEC values in Central America that extended up to 30° magnetic latitude. However, the TEC plots introduced here correspond to K_p values less than 3°. These TEC features were detected almost every day between 8 May and 10 September 2010.

Figure 17 shows the result of our empirical model for 22 December. Here, we observe another "apparent" southern crest to be much more intense than the northern crest. In addition, this crest is displaced in latitude by 20° or more at 50°W longitude. The northern crest is displaced only 10° from the magnetic equator. It is interesting to note that the region of high TEC decays at 16 LT and only a typical southern crest of the anomaly is seen afterward. The fact that both regions of high TEC values were seen in two different solstice seasons, in opposite hemispheres and magnetic latitudes >20°, indicates that their origin is not the fountain effect but probably the plasma dynamics of the mid-latitude ionosphere. This anomalous TEC is called

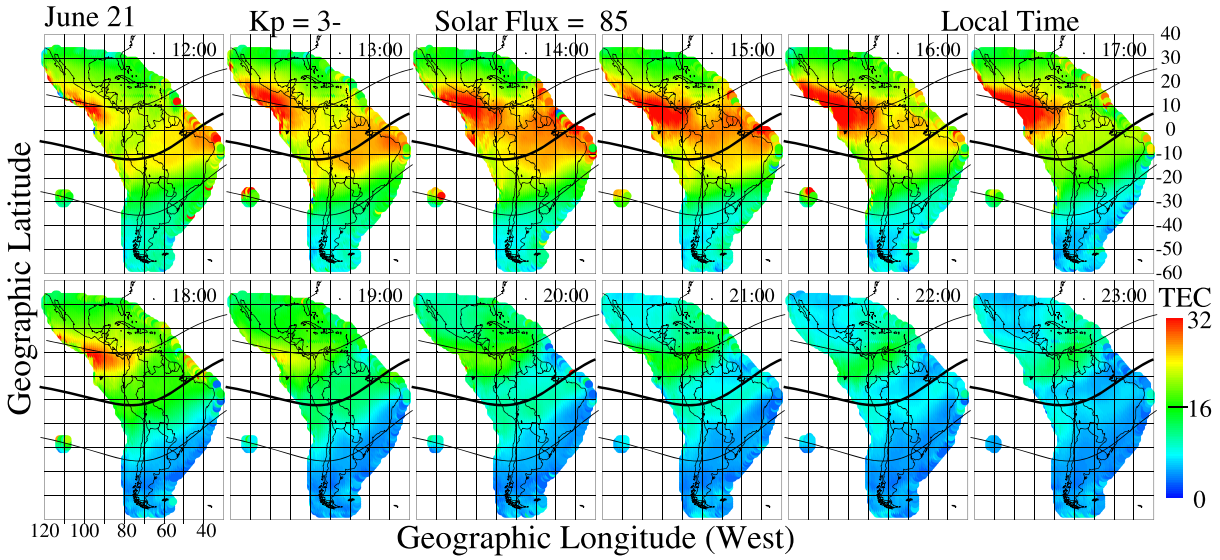

Figure 15. Same as Figure 14 but for 21 June and using the same K_p (3^-) and solar flux values hour-by-hour TEC maps provided by the empirical model (equation (1)). During this season, the highest TEC value is observed over Central America and persists for 6 hr. See text for further comments on this anomalous enhancement.

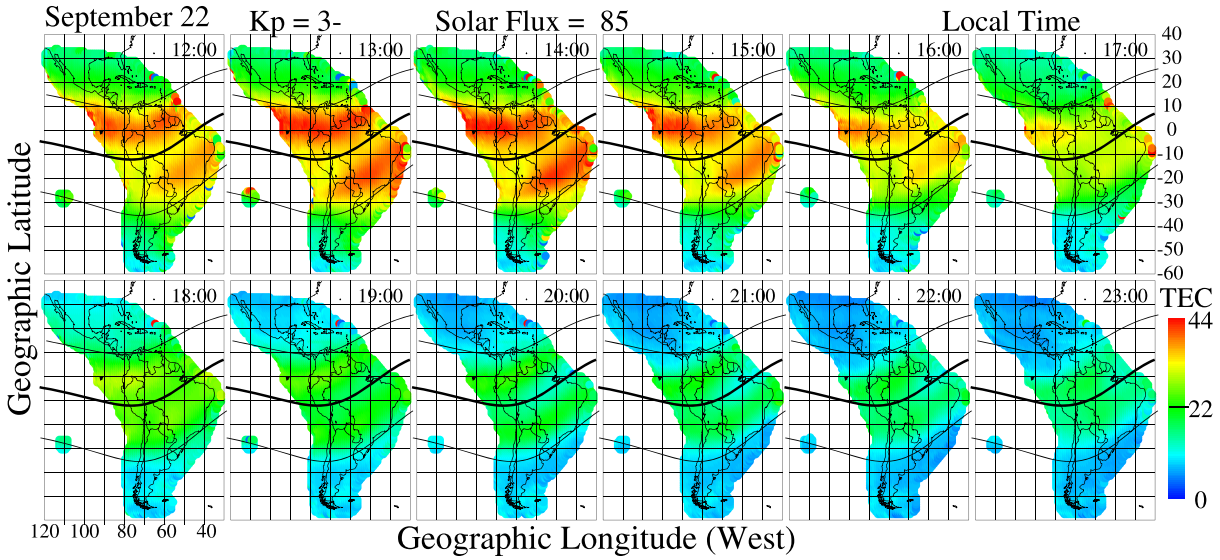

Figure 16. Same as Figure 14 but for 22 September and using the same K_p (3^-) and solar flux values. Similar to Figure 14, which corresponds to March equinox, the prominent feature is the development of a symmetric equatorial anomaly.

tropical TEC enhancement (TTE) because it develops near +23° latitude (tropic of Cancer) in the northern hemisphere and near −23° latitude (tropic of Capricorn) in the southern hemisphere.

4.3. TEC Difference Between Measured and Modeled TEC Values

Figure 18 shows the difference between the TEC values measured on 21 and 22 October 2009 and the TEC values provided by our empirical model using the K_p and solar flux values that prevailed in those days. We have used both periods of typical TEC values that were presented in Figure 3 to assess how well the empirical model can infer the seasonal, K_p, and solar flux trends. Note that Figure 18 displays both positive and negative values on a color scale that has peak values at 44 and −44 TEC units. A close comparison of Figures 3 and 18 indicates that most of the TEC variability has been accounted for by the empirical TEC model.

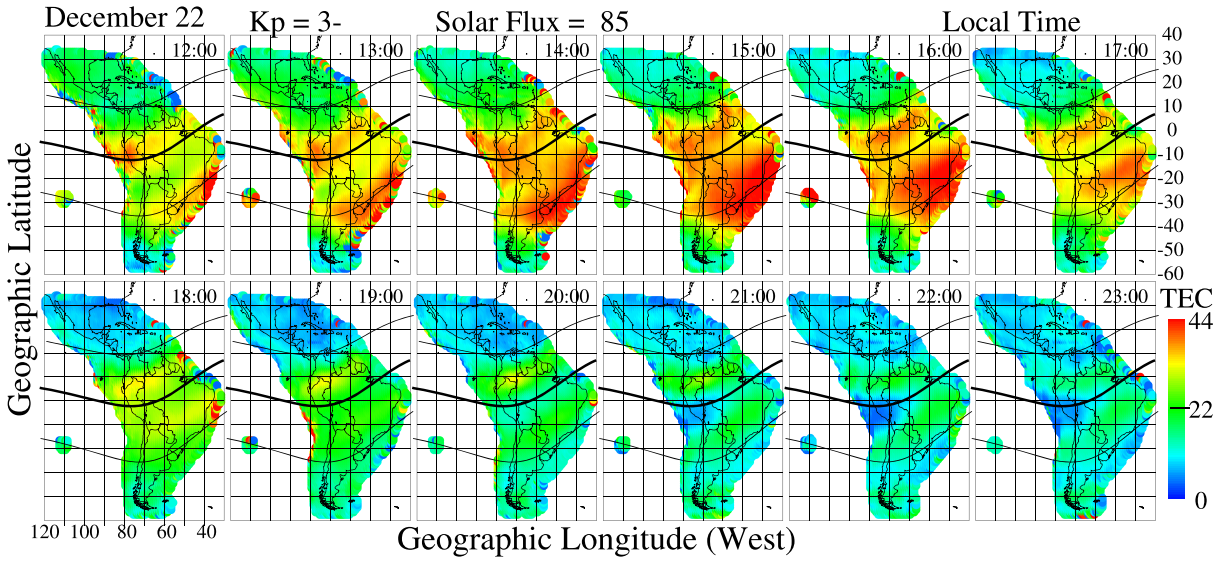

Figure 17. Same as Figure 14 but for 22 December and using the same K_p (3^-) and solar flux values. Note the appearance of a very wide southern crest of the equatorial anomaly that starts at 12 LT and decays at 17 LT. This feature is observed only during the December solstice. See text for further description and relation with the TEC enhancement observed over Central America in Figure 15.

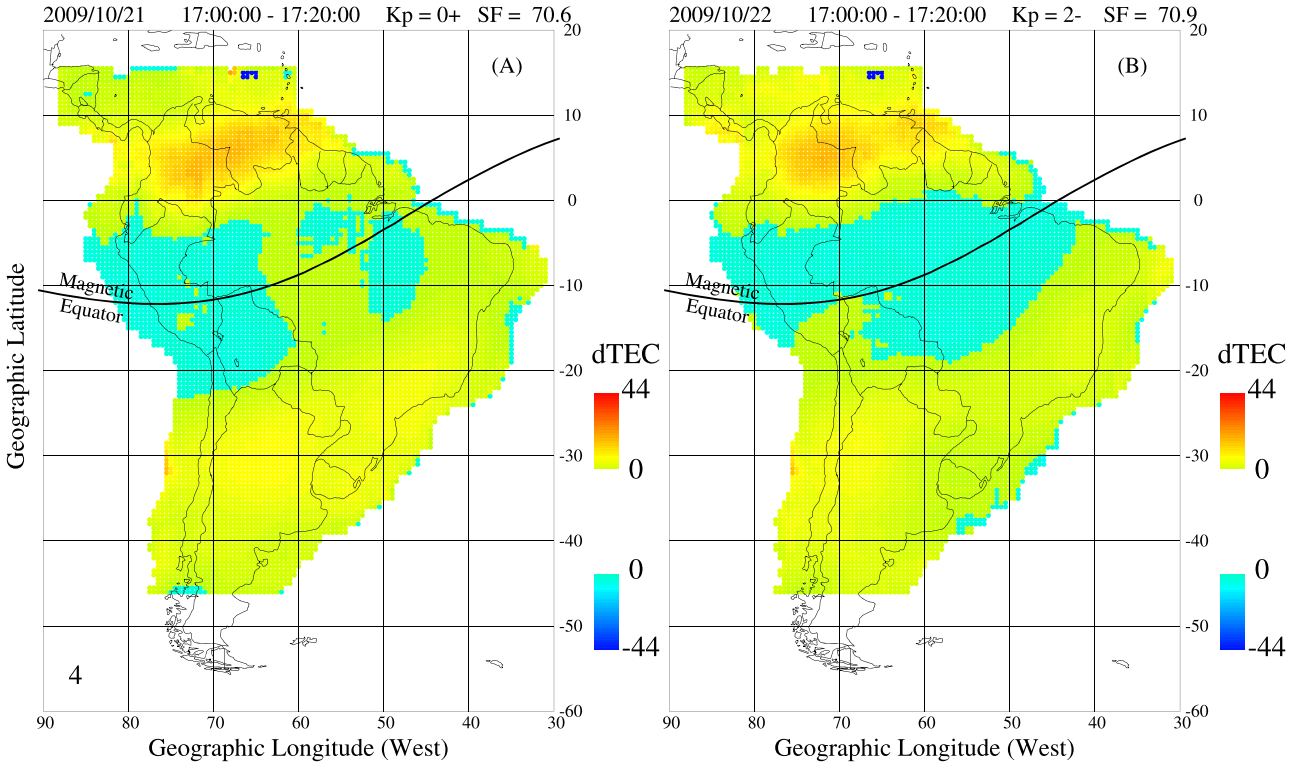

Figure 18. Difference TEC values over South America that were obtained by subtracting measured TEC values and the results of the empirical model (observations − modeling) using the K_p, solar flux, and day number for 21 and 22 October 2009.

However, there remains a small fraction of the northern crest of the equatorial anomaly and a region of positive TEC values near the magnetic equator and between 50° and 60°W longitude in the frame for 21 October 2009 that were likely unique on this day and not represented by the empirical TEC model. The discrepancy between the measured and the fitted values indicates the importance of other physical mechanisms that were not included as drivers in the empirical model (equation (1)). It is suggested that latitudinal changes in the meridional wind and also longitudinal variations in the zonal electric field, driven by the wavenumber 4 and other tide systems, can introduce TEC variations.

5. Discussion

We have described the basic characteristics of the LISN observatory that is presently operating in South America. This observatory is formed by an array of dual-frequency GPS receivers, flux-gate magnetometers, and ionosondes that function continuously and concurrently. Important features of these instruments are their relatively low cost, their versatility, and easy maintenance. The simultaneous operations enhance the diagnostic capabilities in the region, enriching the data sets, and help to find cause-effect relationships between different processes affecting the low-latitude ionosphere. Due to a large number of satellites within the GPS constellation, the LISN GPS receivers are able to measure the TEC values and the S4 scintillation index in several points of the sky simultaneously. Two baselines, each one consisting of a magnetometer pair—one at the magnetic equator and another 6° away—provide the daytime zonal electric fields that drive vertical motions in the F-region ionosphere (Anderson et al., 2004). The ionosondes measure primarily bottom side density profiles, detect E_s layers, diagnose ionospheric tilts, fully probe traveling ionospheric disturbances (TIDs) (Valladares et al., 2017), and under special modes, and processing techniques can give the vertical drifts of the E and F layers.

This publication outlines several aspects of the TEC variability observed in South and Central America that have not been reported before. In addition, the paper illustrates both the spatial and temporal scales of the TEC variability that occur not only during magnetically disturbed periods but equally troublesome during quiet magnetic conditions and during all four seasons. A complete understanding of the role of several

parameters that control the TEC variability is necessary to develop nowcasting and forecasting procedures of the ionospheric density and TEC values. Reliable nowcasting of the ionosphere is now important to provide an accurate real-time model of the ionosphere to any satellite-based augmentation system (SBAS) or a ground-based satellite system (GBAS) that may be operating in South and Central America (Arenas et al., 2016).

The TEC variability contains scales extending between a few hundreds of km and the size of the continent and temporal scales varying between hours and the length of seasons. We emphasize that some of these processes have been addressed before by other authors, and their drivers have been identified and modeled (Khadka et al., 2018). However, other key processes have been revealed by the nature of the spatial coverage of our measurements and will be explained more fully in the next paragraphs.

Near-midnight density and TEC enhancements have been observed by several authors. Balan and Rao (1984) and Balan and Bailey (1995) described the characteristics of TEC enhancements observed in India using signals from the ATS 6 satellite and indicated that the intensity and duration of the TEC enhancements are maxima at equinox and minima in summer. Valladares and Chau (2012) used several networks of GPS receivers operating in South American and the Jicamarca radar to measure the evolution of the density profiles and the variability in latitude, longitude, and duration of the TEC enhancements during an event in 2011 (see their Figure 2b corresponding to 11 March 2011). Computer simulations of near-midnight density/TEC enhancements (Balan & Bailey, 1995) using the Sheffield University plasmasphere-ionosphere model (SUPIM) have indicated the importance of diffusion, $E \times B$ drifts, and neutral winds on the direct and reverse fountain effect. These authors demonstrated that the reverse fountain acts as the main source for the nighttime increase in ionization at low-latitude stations. Their computer simulations implied that convergent meridional winds help plasma to diffuse up the field lines and toward the equator. Valladares and Chau (2012) also stated that the final latitude of the TEC enhancement region depends on the magnitude and direction of the meridional wind and more importantly on the latitude where the meridional winds converge. Figure 8 has shown that the amplitude of the near-midnight TEC enhancement varies as a function of latitude and longitude. Although the latitudinal variability of the reverse fountain effect is basically understood, the longitudinal dependence has not been addressed. The analysis of this type of event will reveal the longitudinal wind variability and help identify the drivers of this type of TEC enhancement. Similar TEC enhancements are observed 20% of the days and under both quiet and disturbed magnetic conditions. The appearance of this type of structure is likely associated with an unusual pattern of winds and electric fields that extend over large distances (e.g., thousands of km) across the continent.

During magnetic storms, prompt penetration electric fields reach the low-latitude ionosphere (Basu et al., 2007; Fejer & Scherliess, 1997). The prompt penetration electric field is eastward (upward drift) in the daytime to the dusk sector and westward in the midnight to the dawn sector (Fejer et al., 1990; Spiro et al., 1978). The periodic wave-type variations presented in Figure 9 are likely associated with a near sunrise westward electric field that lowers the plasma and then makes the plasma diffuse along the field lines. The periodicity of the TEC variations, as seen in the TEC profiles of Ilha Soltera, Brazil at 10 and 13 UT, serves to point out that the prompt penetrating electric field possesses a similar temporal variability. Further study is needed to understand the prominent latitudinal/longitudinal variability of the TEC traces that were observed by different stations on 5 April 2010. This data set can be used to estimate both the large-scale spatial and the temporal variability of the prompt penetration electric field that is associated with the storm condition. The coverage provided by the numerous GPS receivers in South and Central America and the Caribbean region should help to resolve the space-time ambiguity, which commonly affects satellite measurements.

Figures 10 and 12 have shown the TEC distributions corresponding to the equinoctial months of March and September in which the anomaly varies in longitude from an absent southern crest at 70°W to a more symmetric anomaly at 50°W. This important feature of the low-latitude ionosphere over South America can be explained by the pattern of the meridional winds that prevail during the equinoxes and the offset of the geographic and magnetic equator in this region (Khadka et al., 2018).

During the solstices, the declination of the Earth's magnetic field becomes an important parameter to consider. At 70°W, the magnetic declination is almost zero but becomes 20° westward at 50°W. During the June solstice, the amplitude of TEC values is smaller than other seasons; they are only ~50% of the TEC observed in the equinoxes. The smaller TEC value is the result of the smaller vertical drift, the early

reversal, and the absence of pre-reversal enhancement that has been observed with the Jicamarca radar and at this longitude sector with LEO satellites (Fejer et al., 1991; Pacheco et al., 2010). As the F-region stays at lower altitudes during the June solstice, they are greatly affected by recombination. Figure 11 has also shown a highly asymmetric EIA containing a dominant northern crest at all three longitude sectors. Similar crest asymmetry was found by Tulasi Ram et al. (2009) during the northern hemisphere summer and afternoon local time hours. These authors also observed a strong EIA crest in the winter hemisphere during pre-noon hours. We did not observe a dominant crest in the winter hemisphere during the pre-noon hours probably due to the inherent nature of the TEC measurements that integrate into altitude, and thin F layers do not produce a significant increase in TEC values. During the December solstice, the anomaly is symmetric at 70°W, but the southern crest becomes dominant at 50°W. During this season the EIA is more intense than the June solstice anomaly. It is indicated that during the December solstice, the solar terminator aligns with the declination of the field lines in the Brazilian sector creating larger vertical velocities (Abdu et al., 1981; Tsunoda, 1985).

The peculiar variability of the TEC distributions presented in Figures 10–13 has been compared with the maps of the TEC empirical model to understand the control that the solar flux, the K_p index, the seasons, and likely other factors can create the intense variability of the TEC profiles. In 2009 the average solar flux level and the K_p index were 71 units and 2° respectively, making Figures 10–13 representatives of low solar flux and quiet magnetic conditions. Figures 14–17 display the model results for K_p equal to 3^- and a solar flux equal to 85 units. A careful comparison of these two sets of figures for both equinoctial seasons reveals that the anomaly is highly asymmetric, mainly no southern crest in the Peruvian sector (i.e., at all longitudes west of 60°W). East of 60°W, and in the Brazilian sector, the anomaly becomes symmetric, again, in agreement with the monthly averages of Figures 10 and 12. We also generated plots similar to Figures 14–17 for higher solar fluxes and determined that the anomaly becomes more symmetric across the South American continent when the solar flux index is higher than 100 units. It was mentioned above that the meridional wind introduces an asymmetry in the amplitude of the crests by transporting plasma up to the field lines and sometimes across the magnetic equator. In addition, it is known that the vertical drift, the driver of the fountain effect, and then the equatorial anomaly increase when the solar flux is larger (Fejer et al., 1999). This fact makes the anomaly become more pronounced containing higher peaks and a deeper trough. These observations make us conclude that the meridional wind is able to control the characteristics of the anomaly when the equatorial vertical plasma drift is small, and the anomaly is not fully developed.

Figure 15 displays the result of the empirical model for the June solstice in which TEC values are smaller than the TEC observed in other seasons. These TEC values are in agreement with Figure 11. Figure 15 also provides the daily variability of the TEC enhancement seen over Central America and at tropical latitudes (magnetic latitude >20°). The tropical enhancement lasts between 12 and 17 LT hours and extends between 110° and 80°W longitude. It is worth mentioning that the field of view of our measurements ends at 110° and likely this type of TEC enhancement extends further to the West. Figure 15 also reveals three key characteristics of the TEC enhancements: (1) it decays when the zonal wind typically reverses from westward to eastward (17–18 LT) (Hedin et al., 1991). (2) The TEC enhancements occur at longitudes where the magnetic declination is eastward in the northern hemisphere and westward in the southern hemisphere. (3) The eastern end of the TTE region coincides with the region where the declination of the magnetic field line becomes orientated in a north-south direction. The presence of the TTE region in the results of the empirical model implies that this feature occurs quite frequently during the June solstice and for all levels of solar flux and for all K_p conditions.

Figure 17 shows TEC maps for the December solstice in which an "apparent" much wider southern crest is formed by a combination of the anomaly and a region of tropical TEC enhancement. This region develops near 12 LT and decays at 17 LT. However, the part that belongs to the southern crest of the anomaly persists for a few more hours. The region of enhanced TEC values is quite similar to the region of TTE detected during the June solstice in the Central American region as it decays at longitudes where the magnetic declination is no longer directed westward; it is active only in the afternoon hours, and it develops for low and high solar flux values.

We believe that both regions of TTE—one observed over Central America during the June solstice and the second one seen over Southern Brazil during the December solstice—have similar origins. The enhanced

plasma has its sources at poleward latitudes, and it is transported equatorward and up the field lines by the meridional wind to higher altitudes that contain smaller recombination rates and longer lifetimes. It is noted that the upward motion of the plasma along the field lines is not only produced by the meridional wind that maximizes during the solstice but it is also augmented by the afternoon westward zonal wind in regions of non-zero magnetic declination. In this view, the eastward declination in Central America and the westward declination in the southern part of Brazil are key to produce the TTEs that have been detected. We also mention that the large changes in magnetic declination that are present across the South American continent make this the only region on Earth to make it possible to develop this unique type of TEC distribution.

6. Conclusions

Figures 3–17 have shown the pronounced TEC variability that exists in the low-latitude ionosphere over South America. As indicated above, TEC values observed over Central American and the Caribbean region have also been included for the year 2010 to assess the variability in those regions. We did not expect to find a region of high TEC values in Central America at magnetic latitudes above 20° during the June solstice. Similar high TEC values were found at magnetic latitudes less than −20°, extending in the southern coast of Brazil and in the northern coast of Argentina but during the December solstice. These TEC enhancements extended up to latitudes larger than 25° and were observed during both magnetically active and quiet times. Based on this fact, we ruled out the possibility that the super-fountain effect was the driving mechanism of the tropical latitude plasma enhancement. We postulate that this type of TEC enhancement is produced by a combination of two factors: the magnetic declination and the westward zonal wind that prevails in these regions during the afternoon hours. The component of the zonal wind along the field line augmented with a meridional wind directed equatorward is able to move the plasma equatorward along field lines, lifting the plasma, and reducing their recombination rate. The TTE exists during hemisphere summer times when the local density is high enough to create enhancements.

We have also developed a numerical empirical model of the TEC over South and Central America that can be used to provide the basic TEC distributions of the ionosphere. However, it is also concluded that there exist electric fields and winds containing scale sizes of thousands of km that are embedded within the continent that need to be accounted for to have a better understanding of the TEC variability and a more precise representation of the TEC. Then, it is imperative to consider the inputs from the lower thermosphere in the form of tides, planetary waves, and atmospheric gravity waves to fully resolve the sources of the TEC variability. It is also essential to estimate the energy and momentum inputs originated from the lower parts of the atmosphere (Fuller-Rowell et al., 2008; Hagan et al., 2001; Rishbeth, 2006). Although not shown in this report, we are aware that atmospheric gravity waves in the form of TIDs and plasma depletions contribute to increasing the variability of the TEC maps. The contribution of TIDs is commonly less than two TEC units, but TEC depletions can be as high as 15 to 20 TEC units.

As we move to years of high solar activity, it is expected that the number density and then TEC values over South and Central America will intensify and create many opportunities to observe the drivers of the ionospheric variability. The TEC values measured with the LISN network and several other arrays of GPS receivers that operate in South America have proved to be a formidable database to study the ionosphere and can be used as a source for real-time data ingestion capable of deriving the electric fields, neutral winds, and waves that drive the low- and mid-latitude ionospheres.

Acknowledgments
The authors thank Robert Sheehan for his helpful comments and suggestions on the paper. We would like to thank the International GNSS Service (IGS), Geocentric Reference System for the Americas (SIRGAS), and Dr. Michael Bevis from Ohio State University - Central and Southern Andes GPS Project (OSU-CAP) for providing GPS data. Dr. Hector Mora from the Colombian Geological Survey (CGS) provided RINEX files from the stations at Cucuta, Rioacha, Corozal, and Bahia Solano in Colombia. One of the authors, Dr. Valladares, was partially supported by National Science Foundation (NSF) Grants AGS-1552161, AGS-1563025, and AGS-1724133 and Office of Naval Research (ONR) Contract N-00014-17-1-2157. The Low Latitude Ionospheric Sensor Network (LISN) is a project led by the University of Texas at Dallas in collaboration with the Geophysical Institute of Peru, the Universidad Nacional de Colombia, and other institutions that provide information in benefit of the space weather scientific community. We thank all organizations and persons that are supporting and operating receivers under the LISN project. All TEC values that were used to calculate the statistics and produce the plots presented in Figures 2 are available and can be downloaded online (https://lisn.igp.gob.pe).

References

Abdu, M. A., Bittencourt, J. A., & Batista, I. S. (1981). Magnetic declination control of the equatorial F region dynamo electric field development and spread F. *Journal of Geophysical Research*, *86*(A13), 11,443–11,446. https://doi.org/10.1029/JA086iA13p11443

Abdu, M. A., de Paula, E. R., Batista, I. S., Reinisch, B. W., Matsuoka, M. T., Camargo, P. O., et al. (2008). Abnormal evening vertical plasma drift and effects on ESF and EIA over Brazil-South Atlantic sector during the 30 October 2003 superstorm. *Journal of Geophysical Research*, *113*, A07313. https://doi.org/10.1029/2007JA012844

Anderson, D., Anghel, A., Chau, J., & Veliz, O. (2004). Daytime vertical $\mathbf{E} \times \mathbf{B}$ drift velocities inferred from ground-based magnetometer observations at low latitudes. *Space Weather*, *2*(11). https://doi.org/10.1029/2004SW000095

Appleton, E. V. (1946). Two anomalies in the ionosphere. *Nature*. Nature Publishing Group. https://doi.org/10.1038/157691a0.

Arenas, J., Sardón, E., Sainz, A., Ochoa, B., & Magdaleno, S. (2016). Low-latitude ionospheric effects on SBAS. *Radio Science*, *51*, 603–618. https://doi.org/10.1002/2015RS005863

Balan, N., & Bailey, G. J. (1995). Equatorial plasma fountain and its effects: Possibility of an additional layer. *Journal of Geophysical Research*, *100*(A11), 21,421–21,432. https://doi.org/10.1029/95JA01555

Balan, N., & Rao, P. B. (1984). Relationship between nighttime total electron content enhancements and VHF scintillations at the equator. *Journal of Geophysical Research*, *89*(A10), 9009–9013. https://doi.org/10.1029/JA089iA10p09009

Basu, S., Basu, S., Rich, F. J., Groves, K. M., MacKenzie, E., Coker, C., et al. (2007). Response of the equatorial ionosphere to prompt penetration electric fields during intense magnetic storms. *Journal of Geophysical Research*, *112*, A08308. https://doi.org/10.1029/2006JA012192

Eccles, V., Rice, D. D., Sojka, J. J., Valladares, C. E., Bullett, T., & Chau, J. L. (2011). Lunar atmospheric tidal effects in the plasma drifts observed by the low-latitude ionospheric sensor network. *Journal of Geophysical Research*, *116*, A07309. https://doi.org/10.1029/2010JA016282

Eccles, J. V., St. Maurice, J. P., & Schunk, R. W. (2015). Mechanisms underlying the prereversal enhancement of the vertical plasma drift in the low-latitude ionosphere. *Journal of Geophysical Research: Space Physics*, *120*(6), 4950–4970. https://doi.org/10.1002/2014JA020664

Fejer, B. G., de Paula, E. R., Gonzalez, S. A., & Woodman, R. F. (1991). Average vertical and zonal F region plasma drifts over Jicamarca. *Journal of Geophysical Research*, *96*(A8), 13,901–13,906. https://doi.org/10.1029/91JA01171

Fejer, B. G., Kelley, M. C., Senior, C., de la Beaujardiere, O., Holt, J. A., Tepley, C. A., et al. (1990). Low- and mid-latitude ionospheric electric fields during the January 1984 GISMOS Campaign. *Journal of Geophysical Research*, *95*(A3), 2367–2377. https://doi.org/10.1029/JA095iA03p02367

Fejer, B. G., Olson, M. E., Chau, J. L., Stolle, C., Lühr, H., Goncharenko, L. P., et al. (2010). Lunar-dependent equatorial ionospheric electrodynamic effects during sudden stratospheric warmings. *Journal of Geophysical Research*, *115*, A00G03. https://doi.org/10.1029/2010JA015273

Fejer, B. G., & Scherliess, L. (1997). Empirical models of storm time equatorial zonal electric fields. *Journal of Geophysical Research*, *102*(A11), 24,047–24,056. https://doi.org/10.1029/97JA02164

Fejer, B. G., Scherliess, L., & de Paula, E. R. (1999). Effects of the vertical plasma drift velocity on the generation and evolution of equatorial spread *F*. *Journal of Geophysical Research*, *104*(A9), 19,859–19,869. https://doi.org/10.1029/1999JA900271

Fuller-Rowell, T. J., Akmaev, R. A., Wu, F., Anghel, A., Maruyama, N., Anderson, D. N., et al. (2008). Impact of terrestrial weather on the upper atmosphere. *Geophysical Research Letters*, *35*(9), L09808. https://doi.org/10.1029/2007GL032911

Hagan, M., Roble, R., & Hackney, J. (2001). Migrating thermospheric tides. *Journal of Geophysical Research*, *106*(A7), 12,739–12,752. https://doi.org/10.1029/2000ja000344

Hagan, M. E., Maute, A., Roble, R. G., Richmond, A. D., Immel, T. J., & England, S. L. (2007). Connections between deep tropical clouds and the Earth's ionosphere. *Geophysical Research Letters*, *34*(20), L20109. https://doi.org/10.1029/2007GL030142

Hanson, W. B., & Moffett, R. J. (1966). Ionization transport effects in the equatorial F region. *Journal of Geophysical Research*, *71*(23), 5559–5572. https://doi.org/10.1029/JZ071i023p05559

Hedin, A. E., Biondi, M. A., Burnside, R. G., Hernandez, G., Johnson, R. M., Killeen, T. L., et al. (1991). Revised global model of thermosphere winds using satellite and ground-based observations. *Journal of Geophysical Research*, *96*(A5), 7657–7688. https://doi.org/10.1029/91JA00251

Immel, T. J., Sagawa, E., England, S. L., Henderson, S. B., Hagan, M. E., Mende, S. B., et al. (2006). Control of equatorial ionospheric morphology by atmospheric tides. *Geophysical Research Letters*, *33*(15), L15108. https://doi.org/10.1029/2006GL026161

Khadka, S. M., Valladares, C., Pradipta, R., Pacheco, E., & Condor, P. (2016). On the mutual relationship of the equatorial electrojet, TEC and scintillation in the Peruvian sector. *Radio Science*, *51*(6), 742–751. https://doi.org/10.1002/2016RS005966

Khadka, S. M., Valladares, C. E., Sheehan, R., & Gerrard, A. J. (2018). Effects of the electric field and neutral wind on the asymmetry of equatorial ionization anomaly. *Radio Science*, *53*, 683–697. https://doi.org/10.1029/2017RS006428

Mannucci, A. J., Tsurutani, B. T., Iijima, B. A., Komjathy, A., Saito, A., Gonzalez, W. D., et al. (2005). Dayside global ionospheric response to the major interplanetary events of October 29-30, 2003 "Halloween Storms". *Geophysical Research Letters*, *32*, L12S02. https://doi.org/10.1029/2004GL021467

Pacheco, E. E., Heelis, R. A., & Su, S.-Y. (2010). Quiet time meridional (vertical) ion drifts at low and middle latitudes observed by ROCSAT-1. *Journal of Geophysical Research*, *115*, A09308. https://doi.org/10.1029/2009JA015108

Rideout, W., & Coster, A. (2006). Automated GPS processing for global total electron content data. *GPS Solutions*, *10*(3), 219–228. https://doi.org/10.1007/s10291-006-0029-5

Rishbeth, H. (2006). F-region links with the lower atmosphere? *Journal of Atmospheric and Solar - Terrestrial Physics*, *68*(3-5), 469–478. https://doi.org/10.1016/j.jastp.2005.03.017

Sagawa, E., Immel, T. J., Frey, H. U., & Mende, S. B. (2005). Longitudinal structure of the equatorial anomaly in the nighttime ionosphere observed by IMAGE/FUV. *Journal of Geophysical Research: Space Physics*, *110*(A11), A11302. https://doi.org/10.1029/2004JA010848

Spiro, R. W., Heelis, R. A., & Hanson, W. B. (1978). Ion convection and the formation of the mid-latitude *F* region ionization trough. *Journal of Geophysical Research*, *83*(A9), 4255–4264. https://doi.org/10.1029/JA083iA09p04255

Sridharan, R., Raju, D. P., Raghavarao, R., & Ramarao, P. V. S. (1994). Precursor to equatorial spread-F in OI 630.0 nm dayglow. *Geophysical Research Letters*, *21*(25), 2797–2800. https://doi.org/10.1029/94GL02732

Tsunoda, R. T. (1985). Control of the seasonal and longitudinal occurrence of equatorial scintillations by the longitudinal gradient in integrated *E* region Pedersen conductivity. *Journal of Geophysical Research*, *90*(A1), 447–456. https://doi.org/10.1029/JA090iA01p00447

Tulasi Ram, S., Su, S.-Y., & Liu, C. H. (2009). FORMOSAT-3/COSMIC observations of seasonal and longitudinal variations of equatorial ionization anomaly and its interhemispheric asymmetry during the solar minimum period. *Journal of Geophysical Research*, *114*, A06311. https://doi.org/10.1029/2008JA013880

Valladares, C. E., Basu, S., Groves, K., Hagan, M. P., Hysell, D., Mazzella, A. J. Jr., & Sheehan, R. E. (2001). Measurement of the latitudinal distributions of total electron content during equatorial spread *F* events. *Journal of Geophysical Research*, *106*(A12), 29,133–29,152. https://doi.org/10.1029/2000JA000426

Valladares, C. E., & Chau, J. L. (2012). The low-latitude ionosphere sensor network: Initial results. *Radio Science*, *47*(3). https://doi.org/10.1029/2011RS004978

Valladares, C. E., Eccles, J. V., Basu, S., Schunk, R. W., Sheehan, R., Pradipta, R., & Ruohoniemi, J. M. (2017). The magnetic storms of 3–4 August 2010 and 5–6 August 2011: 1. Ground- and space-based observations. *Journal of Geophysical Research: Space Physics*, *122*, 3487–3499. https://doi.org/10.1002/2016JA023359

Valladares, C. E., Sheehan, R., & Pacheco, E. E. (2017). Observations of MSTIDs over South and Central America. In Fuller-Rowell, Yizengaw, Doherty, & Basu (Eds.), *Ionospheric Space Weather Longitude and hemisphere dependences and Lower Atmosphere Forcing*, *Geophysical Monograph 220* (Chap. 16, First ed., pp. 187–205). John Wiley & Sons, Inc. https://doi.org/10.1002/9781118929216.ch16

Walker, G. O., Ma, J. H. K., & Golton, E. (1994). The equatorial ionospheric anomaly in electron content from solar minimum to solar maximum for South East Asia. *Annales Geophysicae*, *12*(2–3), 195–209. https://doi.org/10.1007/s00585-994-0195-0